Axon-seq decodes the motor axon transcriptome and its modulation in response to ALS

Jik Nijssen[1,3], Julio Aguila Benitez[1,3], Rein Hoogstraaten[1,2], Nigel Kee[1] and Eva Hedlund[1]*

[1] Department of Neuroscience, Karolinska Institutet, Stockholm, 171 77, Sweden

[2] Department of Translational Neuroscience, Brain Center Rudolf Magnus, UMC Utrecht, 3984 CG Utrecht, Netherlands

[3] Co-first authors

* To whom correspondence should be addressed. Tel: 0046 (0) 852488784; Email: Eva.Hedlund@ki.se

Present Address: Eva Hedlund, Department of Neuroscience, Karolinska Institutet, 171 77, Stockholm, Sweden

ABSTRACT

Spinal motor axons traverse large distances to innervate target muscle, and thus require local control of cellular events for proper functioning of the distal axon. To interrogate axon-specific processes we developed Axon-seq, a refined method incorporating microfluidic devices and stringent bioinformatic quality controls. Axon-seq demonstrates improved sensitivity and accuracy in whole-transcriptome sequencing of axons compared to previously published studies. Importantly, we show that axon transcriptomes are distinct from those of somas, displaying fewer detected genes and no contaminating astrocytic markers. We identified >5,000 transcripts in stem cell-derived spinal motor axons required for local oxidative energy production and ribosome generation. Axons contained unique transcription factor mRNAs, e.g. Ybx1, with implications for local axonal functions. Cross-comparison with peripheral sensory neuron datasets identified a common axon transcriptome consisting of 1,750 mRNAs, as well as 396 mRNAs unique to motor axons, which included genes for ribogenesis, vesicle transport and mRNA splicing. As motor axons degenerate in amyotrophic lateral sclerosis (ALS), we investigated their response to the disease-causing $SOD1^{G93A}$ mutation, identifying 121 ALS-dysregulated transcripts. Several of these are implicated in axonal and dendritic outgrowth, including Nrp1, Dbn1, and Nek1, a known ALS-causing gene. In conclusion, Axon-seq proves a robust and improved method for RNA-seq of axons, furthers our understanding of peripheral axon biology, and identifies novel therapeutic targets to maintain neural connectivity in disease.

INTRODUCTION

Spinal motor neurons (MNs) are highly polarized cells. Their somas and associated dendrites are located in the spinal cord, while their axons traverse the body and connect to distal muscle fibers. The large distance between MN somas and their pre-synapse implies that the distal axon must contain a micro-environment able to independently respond to internal and external triggers. Fast-anterograde transport in axons carries vesicles with transmembrane proteins at rates up to 400 mm per day. However, vesicles containing proteins and RNAs travel considerably slower, at 0.1-10 mm per day

(Lasek et al., 1984). Thus, protein transport alone would not suffice to sustain the dynamics of an axon and synapse, implying a strong role for local regulation. Indeed, it is well established that local RNA translation in the synapse is important for temporal control of protein synthesis and synaptic plasticity (Holt and Schuman, 2013).

Motor axons and their specialized synapses with muscle, termed neuromuscular junctions (NMJs), are primary targets in the lethal disease amyotrophic lateral sclerosis (ALS). MNs undergo progressive degeneration in ALS, resulting in denervation of muscle, paralysis and ultimately death at 3-5 years post-diagnosis (Swinnen and Robberecht, 2014). Notably, MNs follow a distinct 'dying-back' pattern of degeneration in ALS. Muscle denervation and axonal retraction occur before MN somas in the spinal cord are lost, implying that the NMJ is a highly vulnerable entity of the MN (Comley et al., 2016; Fischer et al., 2004; Valdez et al., 2012). Mutations in several genes such as *SOD1*, *C9orf72*, *TARDBP* (TDP43) and *FUS* have been discovered to cause ALS (DeJesus-Hernandez et al., 2011; Kwiatkowski et al., 2009; Renton et al., 2011; Rosen et al., 1993; Sreedharan et al., 2008; Vance et al., 2009). However, expression of these genes is not restricted to MNs. Why and how they selectively affect MNs in ALS is not clear. Therefore, studying the RNA composition of the distal axon of this vulnerable neuron subtype may illuminate mechanisms driving the specific dying-back degeneration observed in ALS.

Previous efforts to examine axons in isolation *in vitro* have used either cell culture insets, Campenot chambers or microfluidic devices (Boyden, 1962; Campenot, 1977; Taylor et al., 2005). While these are excellent tools for separating axons from somas, residual cross-contamination between the compartments still occurs. In this way, RNA-sequencing efforts aimed at isolating an axonal transcriptome profile (Briese et al., 2016; Gumy et al., 2011; Minis et al., 2014; Rotem et al., 2017; Saal et al., 2014; Taylor et al., 2009) can be easily undermined by a failure to carefully examine the purity of axonal fractions. Due to unappreciated technical difficulties, which are not always acknowledged, axonal fractions can be contaminated with other cellular components or non-neuronal cells. To accurately investigate motor axon mRNA composition and its modulation in ALS we developed Axon-seq, a novel application of our single-cell RNA-preparation technique (Nichterwitz et al., 2016) to microfluidic devices housing mESC derived MNs. In contrast to previous methodologies, Axon-seq does not require RNA isolation, and allows high sensitivity, cost-efficient sequencing from a single microfluidic device. Importantly, Axon-seq utilises a stringent and sensitive bioinformatic quality control step that identifies samples containing trace levels of mRNA from undesired cell somas, effectively eliminating all cellular cross-contamination.

We derive wild type or ALS (mutated $SOD1^{G93A}$) MNs from mouse embryonic stem cells (mESCs) harboring the MN specific reporter Hb9::eGFP. Using Axon-seq, we show that a pure axonal transcriptome consists of roughly 5,000 mRNA species, compared to >15,000 in cell somas. Approximately 10% of the axonal transcriptome was enriched in the axonal versus the somatodendritic compartment, including transcripts involved in energy production, translation and distinct transcription factor mRNAs such as Ybx1. We also reveal 1,750 mRNAs common to peripheral axons by comparing axonal transcriptome data sets across central and peripheral neuron

types. This analysis further decoded a motor axon specific set of 396 mRNAs. Application of Axon-seq to ALS axons uncovered 121 dysregulated transcripts compared to controls, of which several are important for proper neuronal and axonal functioning. Finally, a cross-comparison with axons after *Smn* knockdown, a model for the motor neuron disease spinal muscular atrophy (SMA), revealed that axon guidance receptor neuropilin 1, was downregulated in axons across both MN diseases.

RESULTS

Axon-seq is a refined method that enables RNA sequencing of axons from a single microfluidic device

To investigate transcriptional changes in motor axons in health and ALS we used mESC-derived MNs from a control HB9::eGFP line or cells overexpressing the human mutated SOD1^{G93A} protein. We first confirmed the MN subtype identity of our cultures through bulk RNA sequencing and cross-comparison with single MNs (Nichterwitz et al., 2016). We observed expression of the MN transcription factors Isl1 and Foxp1 in our cultures, similar to single cell data on MNs (Supplemental Fig. S1A). This indicates that MNs of a lateral motor column (LMC) identity, which are patterned by Hox genes, were generated (Dasen et al., 2008). Consistent with this, mRNAs of multiple members of the of Hox1-8 families, which define a cervical to thoracic identity, were detected. Further, expression of the transcription factor Phox2b indicates that a proportion of brainstem MNs are also generated (Supplemental Fig. S1A). After plating cells in microfluidic devices, MN axons were recruited to the vacant chamber by a gradient of GDNF and BDNF (Fig 1A, E). An initial concentration of 50 ng/ml of GDNF/BDNF was followed by a lower concentration of 5ng/ml once axons had crossed the microchannels, as this avoided growth cone collapse (Fig. 1A). The HB9::eGFP reporter signal was detectable in MN axons, as well as in somas where it co-localized with the MN marker Islet1/2 (Fig. 1B). We next stained for *Map2* (Fig. 1C) and *Mapt* (Fig. 1D). In mature neurons, *Map2* labels dendrites, while *Mapt* labels axons (Garner et al., 1988; Litman et al., 1993). The majority of processes extending across the channels were *Mapt*-positive, while a minority were *Map2-positive*, thus axonal processes were enriched in this compartment (Fig 1C-D). MN cultures derived from mESCs also contain interneurons. However, since a very low proportion of GFP-negative (and *Mapt*-positive) axons appeared in the axonal compartment, we here-on refer to axonal preparations as motor axons.

Adding different media volumes to the microfluidic compartments can generate a fluid flow that counteracts diffusion (Mills et al., 2018; Taylor et al., 2005). Using this principle, axonal or somatodendritic samples were lysed without affecting the opposite compartment (Fig. 1F). Further, both compartments could be effectively lysed using 2% triton X-100 in water (Fig. 1E, F), eliminating the need for RNA purification. To boost final RNA concentration and thereby allow sequencing from an individual microfluidic device, we introduced a vacuum centrifugation concentration step, allowing the entire lysate to be used for subsequent cDNA library preparation. Using this cost-efficient approach, we successfully conducted polyA-based RNA-seq on axonal and soma samples from

individual devices using the Smart-seq2 protocol (Picelli et al., 2013) with some minor modifications (Nichterwitz et al., 2016).

We next implemented a crucial bioinformatics-based quality control step (Axon-seq QC) to exclude axon samples displaying trace levels of cross-contamination from the adjacent compartment. First, to be considered for further analysis, samples were required to display at least 300,000 mapped reads, a minimum of 0.4 correlation to at least one other sample, and more than 2,500 detected genes (See Methods). Secondly, we performed principal component analysis (PCA) based on all expressed genes. In this analysis PC1 strongly reflected the number of detected genes, where axonal transcriptomes occupied the lower ranges, and somatodendritic samples occupied the higher ranges (Figure 1H). Three axonal samples displayed 7,539, 8,485 and 7,760 detected genes and occupied mid PC1 ranges. These samples were likely contaminated with one or more somas, and were discarded. Remaining high quality axon samples contained roughly 3,500 detected genes at > 1 RPKM and 5,000 detected genes at > 0.1 RPKM, while somatodendritic samples contained approximately three times these numbers (Fig. 1G). Axonal samples also displayed fewer detected genes when compared to single MNs (Nichterwitz et al., 2016) (Supplemental Fig. S1D). Interestingly, despite this difference, cDNA yield was comparable between axonal samples and single MNs (Supplemental Fig. S1C), suggesting that i) the cDNA yield from all axons in a microfluidic device approaches that of at most only a few cells, and ii) low numbers of detected genes in these samples is not a technical artefact, and is instead a trait unique to the axonal transcriptome. Given that Axon-seq libraries display lower numbers of detected genes than do single cells, a single contaminating cell has potential to drastically and unacceptably alter the readout of an axonal library. We find that consideration of the number of detected genes is perfectly suited to identifying these contaminated samples, allowing further downstream analysis on only pure Axon-seq samples.

After QC, we then sought to compare our Axon-seq dataset to previously published methods, selecting two RNA-seq studies (Supplemental Table S2) that used either cell culture insets (Rotem et al., 2017) or single microfluidic devices (Briese et al., 2016) to isolate motor axon transcriptomes. Both these studies display high quality data and describe enrichment of axonal transcript. Expression of neuronal markers in all samples was visualized in a heatmap, including e.g. neurofilaments, peripherin, *Mapt*, *Gap43* and the glial markers *Gfap*, *Aqp4*, *Eaat1*, *Iba1*, *Ccl3*, *Pdgfra*, *Sox10* and *Mog* (Fig. 1I). This analysis clearly demonstrates that our Axon-seq samples expressed robust levels of neuronal and axonal markers, while being devoid of glial markers (e.g. Gfap, Eaat1, Pdgfra and Sox10), which were in fact present in all previously published axon samples. Furthermore, our axon samples clustered away from somatodendritic and our cross-contaminated axon samples, while axon and soma samples from previously published studies were intermingled (Fig. 1I). Further cross-comparison of our axon samples with a published data derived from purified neuronal samples (Zhang et al., 2014) confirmed their purity (Supplemental Fig. 1B). Importantly, our Axon-seq samples expectedly displayed a far lower number of detected genes than the previously published axon samples (Fig. 1I, top color bar). Thus, samples displaying even small levels of soma contamination were successfully identified through application of Axon-seq QC.

In summary, our analysis demonstrates the importance of extensive QC of axon transcriptome data with particular consideration for the number of detected genes, and presents Axon-seq as a robust and improved method for RNA-seq of pure axonal fractions from a single microfluidic device with sensitivity similar to single cell sequencing.

Axons have a unique transcriptional profile and are particularly enriched in transcripts important for mitochondrial and ribosomal functions

We next sought to compare the transcriptome of the axonal fraction against the somatodendritic fraction. When considering transcripts present in at least 3 out of 5 axonal samples, the axonal transcriptome comprised 4,238 genes (Supplemental Table S3). 10,406 genes were differentially expressed between axons and somas. The majority of these (9,762) were enriched in the soma, while 644 transcripts were axon-enriched (Supplemental Table S4). Moreover, analysis of the top 100 differentially expressed genes in axons and somas respectively, clearly demonstrated that axons are not simply diluted somas, but instead have a unique mRNA profile (Supplemental Fig S1E). Principle component analysis based on all expressed genes clearly distinguished axons from somas, with PC1 explaining 41.7% of the variance (Fig. 2A). The top 20 genes determining PC1-negative loading and thereby axonal identity, included several genes involved in the mitochondrial respiratory chain (*Cox6a1*, *Cox6b1*, *Cox8a*, *Cox4i1*, *Ndufa3*, *Ndufa7*, *Ndufb9*, *Ndufb11*, *Uqcrq*), others in mitochondrial ATP synthesis (*Atp5k*, *Atp5j2*), ribosome subunits and transcriptional elongation (*Rpl41*, *Tceb2*), cytoskeleton organization (*Tmsb10*), copper delivery (*Atox1*) and mRNA splicing (*Ybx1*) (Fig. 2B). The PC1-positive loading (Fig. 2A) was strongly influenced by transcripts present in somas that were completely absent in axons. In total, 2,903 genes were expressed at an average of RPKM > 1 in somas, that were undetectable in axons (Supplemental Fig S1F). Gene set enrichment analysis (GSEA) on axonal enriched genes uncovered pathways related to local translation (Fig. 2C, E), mitochondrial oxidative energy production (Fig. 2D) and nonsense-mediated decay (Fig. 2F). Both nuclear- or mitochondrial encoded transcripts were enriched in axons (Fig. 2G, H), while the ten most abundant axon-enriched transcripts were related to mitochondrial energy production (Fig. 2I). Immunocytochemistry of motor axons demonstrated that also the *Cox6a1* protein, which is part of the electron transport chain, was readily detected in axons (Fig. 2J).

In summary, our data shows that the axons of growing MNs are enriched for mRNAs related to ribosomes and mitochondrial oxidative phosphorylation, a large majority of which are mitochondrially produced. The distal axon compartment can thereby sustain local translation machinery and high energy metabolism, reflecting the enormous energy demands of growing axons.

Motor axons show a unique transcription factor profile

Analysis of the top 50 most prevalent transcription factor mRNAs in each of the two compartments uncovered 16 transcription factors were common to both compartments, including *Ybx1*, *Carhsp1* and *Sub1* (Fig. 3A,B). Notably, the majority of soma-enriched TFs mRNAs were more abundant in somas than most axon-enriched TFs were abundant in axons (Fig. 4B). However, five of the ten most

abundant axonal TF mRNAs were significantly enriched in this compartment compared to somas, including *Ybx1*, *Carhsp1*, *Pbx4*, *Hmga1* and *Zfp580* (Fig. 3C). The enrichment of *Ybx1* (Y-box binding protein 1, $p < 0.001$) (Fig. 3C) was particularly compelling since Ybx1 partakes in e.g. pre-mRNA transcription and splicing, mRNA packaging and regulation of mRNA stability and translation (Lyabin et al., 2014a; Lyabin et al., 2014b). Immunocytochemistry confirmed *Ybx1* protein's localization to motor axons (Fig. 3D), strengthening a possible role for Ybx1 in supporting local regulation of distal axonal cellular processes.

In summary, axons show a unique transcription factor profile which is expected to reflect functions particular to this compartment, and that could potentially function as communication and control signals between somas and their long range axonal projections.

Cross comparison of axonal data sets across neuronal subtypes reveals both motor neuron-enriched and pan-neuronal axon mRNA repertoires

To understand which mRNAs define growing axons in general and which are specific to motor axons, we compared our Axon-seq motor axons with three published axon datasets derived from primary embryonic mouse MNs (Saal et al., 2014), or primary embryonic mouse dorsal root ganglia (DRG) (Gumy et al., 2011; Minis et al., 2014). We selected the top 5,000 expressed transcripts from each dataset. Importantly, more than half (3,172) of the 5,000 genes identified in Axon-seq motor axons were shared with primary motor axons. Of these 3,172 genes, 396 were excluded from DRG axons and are, thereby, motor axon specific (Fig 4A). Each group contained a unique mRNA repertoire, but the four groups also shared 1,750 genes. GO term analysis of these 1,750 pan-axonal genes identified once again biological processes such as translation, electron transport chain, anterograde axonal transport, proteasome-mediated catabolic processes, synaptic vesicle transport and mRNA splicing (Fig. 4B, supplemental table S5). Full gene lists for the common, DRG-specific and MN-specific transcripts can be found in supplemental table S6.

Finally, we conducted STRING analysis on the 396 motor axon-specific and 427 DRG axon-specific transcripts (Fig. 4C, Supplemental Fig S2, 3) to identify possible protein-protein interaction networks. Notably, for motor axons we identified distinct gene clusters involved in ribogenesis, vesicle transport and mRNA splicing(Fig. 4C, Supplemental Fig. S2), putative candidates for selective MN axon function.

In summary, our analyses have identified a general axonal transcriptional signature as well as defined a unique motor axon code which gives clues to function as well as their particular susceptibility in disease.

The ALS-causative mutation SOD1^{G93A} modulates the axonal transcriptome

Motor axons are early pathological targets in the lethal MN disease ALS, where die-back pathology begins in the distal axon. We therefore investigated if overexpression of an ALS causative mutation (*SOD1*^{G93A}) would induce changes in the axonal transcriptome. MNs derived from mESCs

overexpressing human SOD1^{G93A} have high levels of SOD1 protein in somas and axons (Fig. 5A). Axon-seq of SOD1^{G93A} axons identified 4,479.5 ± 1327.7 genes at RPKM > 1 and 6,568.8 ± 2293.1 at RPKM > 0.1 (Supplemental table S7). Human mutant *SOD1* was highly expressed in somas and axons (Fig. 5B) at levels approximately 10-fold higher than mouse *Sod1* (Fig. 5C). Interestingly, mouse *Sod1* mRNA levels were higher in axons than in soma ($p < 0.001$), likely reflecting the important role of this enzyme in converting reactive superoxide radicals produced in the abundant axonal mitochondria. Mutant *SOD1* overexpression resulted in differential expression of 121 genes in axons compared to the control line, of which 96 were upregulated in SOD1^{G93A} axons, while 25 were reduced (Fig. 5D, Supplemental Table S8). Strikingly, all but two of these genes (*Zfand1* and *Zfp688*) were uniquely dysregulated in mutant axons and were not differentially expressed between the control and SOD1^{G93A} soma compartments. Moreover, many of these genes have previously been implicated in general neuronal function as well as in ALS pathology (Fig. 5E). For instance, we found that several transcripts paramount for proper axon function were downregulated or completely absent in SOD1^{G93A} axons, including *Dbn1* (Lin and Koleske, 2010; McIntyre et al., 2010; Sharma et al., 2012), *Nrp1* (neuropilin 1) (Telley et al., 2016) and *Mgrn1* (Upadhyay et al., 2016),. Some transcripts that were upregulated in SOD1^{G93A} axons appear detrimental, including *Adgr1* (Zuko et al., 2016) (Fig. 5E). Additionally, upregulation of some transcripts with ALS could reflect compensatory mechanisms, including *Dhx36* (Bicker et al., 2013), *Nek1* (Kenna et al., 2016), *F3* (contactin 1) (Bizzoca et al., 2009), *Rbpms* (Hornberg et al., 2013) and *Farp1* (Zhuang et al., 2009) (Fig. 5E), that may prevent axon damage or dysfunction in SOD1^{G93A} axons.

Finally, we wanted to elucidate if any of the transcripts that were dysregulated by the SOD1^{G93A} mutation were affected across motor neuron diseases. We therefore compared our RNA sequencing data with a microarray data set on motor axons in which the *Smn* gene was knocked down to model the disease spinal muscular atrophy (Saal et al., 2014). Sixteen transcripts were regulated across the two disease models. However, 15 genes were regulated in the opposite direction between the ALS and the SMA disease models, while one transcript, the axon guidance receptor Neuropilin 1 (*Nrp1*), was down-regulated in both motor neuron disease models (Fig. 5F).

In summary, application of Axon-seq methodology to a mutant *SOD1* overexpression model of ALS identified dysregulation of 121 axonal specific transcripts, some of which appear detrimental, while others may indicate compensatory mechanisms to counteract any induced dysfunction. *Nrp1* was downregulated in motor axons across ALS and SMA disease models and might have implications for pathology.

DISCUSSION

Axonal RNA biology is increasingly implicated in ALS, which recent studies have aimed to address (Briese et al., 2016; Rotem et al., 2017). In this study, we developed Axon-seq, an improved method allowing isolation and interrogation of the transcriptome of distal motor axons. We show that with

careful bioinformatic QC, this cost-effective and sensitive methodology can reliably yield high quality, and pure axonal transcriptomes free of contaminating astrocytic or soma restricted transcripts. We detected >5,000 mRNA transcripts in axons, as opposed to somas, where we detected > 15,000 transcripts. Differential gene expression shows that the axonal compartment is not simply a dilution of the soma compartment, and is instead enriched for mRNAs coding for mitochondrial energy production and ribosomes. This distinct profile reflects the high energy-dependence of growing axons and the importance of local protein translation to react to the local environment. For instance, during axon guidance the growth cone responds to guidance cues through local protein synthesis, which is required for directional turning and collapse response (Campbell and Holt, 2001). In fact, axonal protein synthesis in chick sympathetic axons was shown to account for 5% of the total protein synthesis of the cell (Lee and Hollenbeck, 2003). Furthermore, transcripts for all essential subunits of the proteasome system (*Psma1-7* and *Psmb1-7*) were present in motor axons (Supplemental Table S3). Many regulatory subunits and chaperones were also detected, implying extensive regulation of protein degradation in axons. Given that small amounts of RNA can be translated into multiple protein copies, maintaining in neuronal processes an mRNA pool poised for translation both saves energy, and increases capacity for a rapid response. Moreover, some proteins may be toxic during transport and producing these locally would avoid any detrimental effects (Besse and Ephrussi, 2008; Du et al., 2007).

The two largest groups of mRNAs identified in axons through GO term analysis and gene set enrichment analysis (GSEA) were mitochondrially-encoded mRNAs involved in energy production and mitoribosomes. As mitochondria are abundant in axons, and assuming there exists no bias in soma to axon transport of mitochondrially-encoded RNAs, we speculate that these mRNAs are locally transcribed. This would be consistent with our finding that nuclear encoded mRNAs for energy production, and in particular nuclear encoded ribosomal RNAs, were less abundant in axons compared to mitochondrially encoded genes, and in agreement with previous reports also describing a predominance of mitochondrially encoded genes in DRG axons (Minis et al., 2014). Mitochondria can replicate by fission in peripheral axons (Amiri and Hollenbeck, 2008). a process that would be facilitated by local transcription and translation of mitochondrially encoded proteins Interestingly, our data suggests that in fact the complete mRNA library required for mitochondrial replicative fission and function is present locally in axons, in part through a significant contribution from local axonal transcription.

Transcription factors, induced by local morphogens, define the identity of neurons during early development and are later often required for neuronal survival (Kadkhodaei et al., 2013; Sgado et al., 2006). Particular transcription factors have recently been shown to have functions outside of the cell soma and to be important in neuronal circuitry plasticity, axon pathfinding and neuroprotection (Sugiyama et al., 2008; Torero Ibad et al., 2011; Wizenmann et al., 2009). In fact, multiple studies have identified axonal mRNAs for transcription factors, in addition to nuclear transport machinery and the nuclear envelope, whose local translation and subsequent signaling to the soma appear vital to axon maintenance and survival in injury paradigms (Ben-Yaakov et al., 2012; Cox et al., 2008; Hanz

et al., 2003; Ji and Jaffrey, 2012; Yoon et al., 2012). Axon-seq detected a specific set of transcription factor mRNAs enriched in distal MN axons compared to somas, including the RNA-binding factor *Ybx1*. YBX1 has known roles in binding and stabilizing cytoplasmic mRNAs as well as in regulating translation by affecting the interaction between eukaryotic initiation factors and mRNAs (Lyabin et al., 2014b). YBX1 was also shown to mediate the anterograde axonal transport of transcripts of the mitochondrial protein, Cox4 (Kar et al., 2017). Interestingly, in this function YBX1 was shown to interact with FUS, an RNA binding protein and known ALS-causing gene. We expect that YBX1 and other axonally located transcription factors identified here will emerge as important mediators of communication between somas and axons.

'Dying-back' pathology in vulnerable MNs imply that the distal axonal compartment undergoes pathological changes during ALS. Axon-seq on motor axons harbouring the ALS-causative mutation SOD1^{G93A} uncovered differential expression of 121 mRNAs, several of which are crucial for neuronal function, axon maintenance and growth. For example, a number of the transcripts that were upregulated in SOD1^{G93A} axons appear detrimental, including; *Adgr1*, which can induce apoptosis and cause reduction in neurite outgrowth (Zuko et al., 2016). Furthermore, multiple transcripts that are important for axon function were downregulated or absent in SOD1^{G93A} axons, including; *Dbn1* which is important for axon initiation, growth and guidance, (Lin and Koleske, 2010; McIntyre et al., 2010; Sharma et al., 2012), *Nrp1* (Neuropilin 1) which is a semaphorin receptor involved in both axon guidance and subcellular target recognition (Telley et al., 2016); and *Mgrn1* a ubiquitin-ligase, which appears important for mitochondrial function and neuronal survival (Upadhyay et al., 2016). *Mgrn1* has previously been shown to be downregulated in SOD1 mice, as well as being recruited to SOD1-positive inclusions (Chhangani et al., 2016). *Nrp1* is important for limb innervation (Huettl et al., 2011), and it's downregulation here would align with a loss of NMJ function It is noteworthy that *Nrp1* was downregulated in motor axons across SMA and ALS disease models. This indicates that NRP1 might be a target that could be modulated in both diseases with potential beneficial results.

Interestingly, the SOD1 mutation also caused an upregulation of transcripts that could be beneficial to axons, possibly through compensatory mechanisms aimed at preventing axon damage or dysfunction that are in play in SOD1^{G93A} axons. Induced transcripts with potential beneficial properties included; *Dhx36*, an ATP-dependent helicase, which mediates dendritic localization of miRNA 134 with consequent effects on synaptic protein synthesis and plasticity (Bicker et al., 2013); *F3* (contactin 1), a cell adhesion molecule involved in neurite outgrowth (Bizzoca et al., 2009); *Rbpms*, an RNA-binding protein with importance for RNA-granule localization and dendritic arbor complexity, as shown in retinal ganglion cells (Hornberg et al., 2013); *Farp1*, a marker for LMC MNs which positively regulates dendrite growth (Zhuang et al., 2009); *Nek1*, which has a putative role in microtubule stability, neuronal morphology and axon polarity. Interestingly, loss of function variants of *NEK1* confer susceptibility to ALS in humans (Kenna et al., 2016).

In summary, we have developed Axon-seq, a refined method with high sensitivity for RNA sequencing on axons, which contains crucial bioinformatics quality control steps to identify high quality and improved purity axon transcriptomes. Using Axon-seq, we demonstrate that motor axons contain a

distinct repertoire of mRNAs, typified by a lower number of detected genes when compared to somas, and high enrichment for transcripts required for local energy production and protein translation. We further show that a subset of these is shared with axons of other neuronal types, underlining their importance in general axonal biology. Finally, motor axons expressing ALS-causative $SOD1^{G93A}$ displayed both down- and upregulation of key transcripts involved in axonal growth and guidance, as well as neuronal survival. These differences likely represent pathological as well as compensatory processes induced by the mutation.

Due to its robustness, sensitivity and cost effectiveness, we anticipate that Axon-seq will have broad utility in the study of RNA dynamics in any polarized cell. The method will be particularly useful for the study of human neuronal processes in stem cell-derived *in vitro* systems. Thus far, axons of human stem cell-derived glutamatergic neurons have been isolated in microfluidic devices and screened using microarrays (Bigler et al., 2017), but not using more advanced RNA-seq methods. Microfluidic devices have also been used to investigate axonal trafficking deficits and axonal degeneration in stem cell-derived MNs from ALS patients (Naumann et al., 2018). In such settings, Axon-seq provides an additional layer of transcriptome-wide data, facilitating identification of the transcriptional networks underlying pathological changes in human motor axons.

EXPERIMENTAL PROCEDURES

Culturing of motor neurons in microfluidic devices

MNs were resuspended at 100,000 cells/µl and loaded into coated microfluidic devices (SND150, Xona microfluidics). Neural differentiation media was supplemented with 10 ng/ml GDNF, BDNF, CNTF and NT3, 200µM of ascorbic acid (Sigma-Aldrich), 100nM RA and 2µM 5-Fluoro-2'-deoxyuridine (5FdU, Sigma-Aldrich). The axonal compartment was filled with media containing 50ng/ml of GDNF and BDNF to facilitate axonal recruitment. Media in the devices was changed daily and after 2 days, GDNF and BDNF concentrations in the axonal compartment were reduced to 5 ng/ml. In the motor neuron compartment, trophic factor concentrations were doubled from this point onwards to 20 ng/ml and RA was no longer included in the MN media.

Harvesting, library preparation and sequencing

Cultures were harvested after one week in the microfluidic devices using 2% triton X-100 (in water) and 1.5U of RNAse inhibitor (Takara). Lysis solution (75 µl) was flushed through the compartments, collected and snap-frozen on dry ice. Prior library preparation, the volume of axonal samples was reduced from ~75µl to 12-15µl using a concentrator (Eppendorf) and 10µl of the lysate used for reverse transcription. 5µl of the lysates from somatodendritic samples were directly used for the RT reaction, carried out in a final volume of 10 µl. Further steps were carried out as described (Nichterwitz et al., 2016) and samples sequenced on Illumina HiSeq2000 and -2500 platforms.

RNA-seq data processing and analysis

Reads were mapped to the mm10 mouse reference genome and the human SOD1 gene locus (hg38/GRCh38) with HISAT version 2.0.3 (Kim et al., 2015). Aligned reads were extracted and assigned using the GenomicAlignments package (version 1.8.4, Lawrence et al., 2013) in R, with the function summarizeOverlaps, mode set to 'union'. Normalized RPKM values were calculated using gene exon lengths from mm10 Ensembl version GRCm38.87 for mouse. Basic sequencing quality control was performed. Exclusion criteria were: < 300,000 (axons) or < 500,000 (somas) uniquely mapped reads, Spearman correlation to other samples < 0.4 or < 2,500 genes expressed at RPKM > 0.1. To ensure that high-quality axonal samples were not biologically cross-contaminated with material from cell somas, during the cell seeding process or the lysis, we conducted Spearman correlation, unsupervised hierarchical clustering and PCA of all samples that passed initial QC. Axonal samples that clustered with soma samples in these analyses were removed. For the control Hb9::GFP mESC line, MN soma samples (N=13) originated from six independent differentiation experiments and axon samples (N=8) from three independent experiments. For the $SOD1^{G93A}$-overexpressing mESC line, MN soma samples (N=10) originated from six independent differentiation experiments and axon samples (N=4) from two independent experiments.

ACCESSION NUMBERS

The original RNA sequencing data from this study are available at the NCBI Gene Expression Omnibus (GEO, http://www.ncbi.nlm.nih.gov/geo/) under accession number GSE107402.

SUPPLEMENTAL INFORMATION

Supplementary Data and Experimental Procedures are available online.

ACKNOWLEDGEMENTS

We would like to thank Mattias Karlen for his excellent work in creating the schematic for figure 1. This work was supported by grants from the Swedish Research Council [2016-02112]; EU Joint Programme for Neurodegenerative Disease (JPND) [529-2014-7500]; the Strategic Research Programme in Neuroscience; Karolinska Institutet; and Magnus Bergvalls stiftelse [2015-00783, 2016-01531] to E.H. J.A.B. is supported by a postdoctoral fellowship from the Swedish Society for Medical Research (SSMF) and N.K. is supported by a postdoctoral fellowship from the Swedish Brain Foundation. Funding for open access charge: Swedish Research Council [2016-02112] to E.H.

AUTHOR CONTRIBUTIONS

E.H. conceived the project. J.N., J.A.B and E.H. designed experiments. J.N., J.A.B and R.H. acquired data. J.N., J.A.B, R.H., N.K. and E.H. analyzed data. E.H. supervised the project. J.N. and E.H. wrote the manuscript with the help of J.A.B. and N.K. All authors edited and gave critical input on the manuscript.

CONFLICT OF INTEREST

The authors declare that there are no conflicts of interest.

REFERENCES

Allodi, I., and Hedlund, E. (2014). Directed midbrain and spinal cord neurogenesis from pluripotent stem cells to model development and disease in a dish. Front Neurosci *8*, 109.

Amiri, M., and Hollenbeck, P.J. (2008). Mitochondrial biogenesis in the axons of vertebrate peripheral neurons. Dev Neurobiol *68*, 1348-1361.

Ben-Yaakov, K., Dagan, S.Y., Segal-Ruder, Y., Shalem, O., Vuppalanchi, D., Willis, D.E., Yudin, D., Rishal, I., Rother, F., Bader, M.*, et al.* (2012). Axonal transcription factors signal retrogradely in lesioned peripheral nerve. EMBO J *31*, 1350-1363.

Besse, F., and Ephrussi, A. (2008). Translational control of localized mRNAs: restricting protein synthesis in space and time. Nat Rev Mol Cell Biol *9*, 971-980.

Bicker, S., Khudayberdiev, S., Weiss, K., Zocher, K., Baumeister, S., and Schratt, G. (2013). The DEAH-box helicase DHX36 mediates dendritic localization of the neuronal precursor-microRNA-134. Genes Dev *27*, 991-996.

Bigler, R.L., Kamande, J.W., Dumitru, R., Niedringhaus, M., and Taylor, A.M. (2017). Messenger RNAs localized to distal projections of human stem cell derived neurons. Sci Rep *7*, 611.

Bizzoca, A., Corsi, P., and Gennarini, G. (2009). The mouse F3/contactin glycoprotein: structural features, functional properties and developmental significance of its regulated expression. Cell adhesion & migration *3*, 53-63.

Boyden, S. (1962). The chemotactic effect of mixtures of antibody and antigen on polymorphonuclear leucocytes. J Exp Med *115*, 453-466.

Briese, M., Saal, L., Appenzeller, S., Moradi, M., Baluapuri, A., and Sendtner, M. (2016). Whole transcriptome profiling reveals the RNA content of motor axons. Nucleic Acids Res *44*, e33.

Campbell, D.S., and Holt, C.E. (2001). Chemotropic responses of retinal growth cones mediated by rapid local protein synthesis and degradation. Neuron *32*, 1013-1026.

Campenot, R.B. (1977). Local control of neurite development by nerve growth factor. Proc Natl Acad Sci U S A *74*, 4516-4519.

Chhangani, D., Endo, F., Amanullah, A., Upadhyay, A., Watanabe, S., Mishra, R., Yamanaka, K., and Mishra, A. (2016). Mahogunin ring finger 1 confers cytoprotection against mutant SOD1 aggresomes and is defective in an ALS mouse model. Neurobiol Dis *86*, 16-28.

Comley, L.H., Nijssen, J., Frost-Nylen, J., and Hedlund, E. (2016). Cross-disease comparison of amyotrophic lateral sclerosis and spinal muscular atrophy reveals conservation of selective vulnerability but differential neuromuscular junction pathology. J Comp Neurol *524*, 1424-1442.

Cox, L.J., Hengst, U., Gurskaya, N.G., Lukyanov, K.A., and Jaffrey, S.R. (2008). Intra-axonal translation and retrograde trafficking of CREB promotes neuronal survival. Nat Cell Biol *10*, 149-159.

Dasen, J.S., De Camilli, A., Wang, B., Tucker, P.W., and Jessell, T.M. (2008). Hox repertoires for motor neuron diversity and connectivity gated by a single accessory factor, FoxP1. Cell *134*, 304-316.

DeJesus-Hernandez, M., Mackenzie, I.R., Boeve, B.F., Boxer, A.L., Baker, M., Rutherford, N.J., Nicholson, A.M., Finch, N.A., Flynn, H., and Adamson, J. (2011). Expanded GGGGCC hexanucleotide repeat in noncoding region of C9ORF72 causes chromosome 9p-linked FTD and ALS. Neuron *72*, 245-256.

Du, J., Tran, T., Fu, C., and Sretavan, D.W. (2007). Upregulation of EphB2 and ephrin-B2 at the optic nerve head of DBA/2J glaucomatous mice coincides with axon loss. Invest Ophthalmol Vis Sci *48*, 5567-5581.

Fischer, L.R., Culver, D.G., Tennant, P., Davis, A.A., Wang, M., Castellano-Sanchez, A., Khan, J., Polak, M.A., and Glass, J.D. (2004). Amyotrophic lateral sclerosis is a distal axonopathy: evidence in mice and man. Exp Neurol *185*, 232-240.

Garner, C.C., Tucker, R.P., and Matus, A. (1988). Selective localization of messenger RNA for cytoskeletal protein MAP2 in dendrites. Nature *336*, 674-677.

Gumy, L.F., Yeo, G.S., Tung, Y.C., Zivraj, K.H., Willis, D., Coppola, G., Lam, B.Y., Twiss, J.L., Holt, C.E., and Fawcett, J.W. (2011). Transcriptome analysis of embryonic and adult sensory axons reveals changes in mRNA repertoire localization. RNA *17*, 85-98.

Guo, W., Naujock, M., Fumagalli, L., Vandoorne, T., Baatsen, P., Boon, R., Ordovas, L., Patel, A., Welters, M., Vanwelden, T*., et al.* (2017). HDAC6 inhibition reverses axonal transport defects in motor neurons derived from FUS-ALS patients. Nature communications *8*, 861.

Hanz, S., Perlson, E., Willis, D., Zheng, J.Q., Massarwa, R., Huerta, J.J., Koltzenburg, M., Kohler, M., van-Minnen, J., Twiss, J.L*., et al.* (2003). Axoplasmic importins enable retrograde injury signaling in lesioned nerve. Neuron *40*, 1095-1104.

Holt, C.E., and Schuman, E.M. (2013). The central dogma decentralized: new perspectives on RNA function and local translation in neurons. Neuron *80*, 648-657.

Hornberg, H., Wollerton-van Horck, F., Maurus, D., Zwart, M., Svoboda, H., Harris, W.A., and Holt, C.E. (2013). RNA-binding protein Hermes/RBPMS inversely affects synapse density and axon arbor formation in retinal ganglion cells in vivo. J Neurosci *33*, 10384-10395.

Huettl, R.E., Soellner, H., Bianchi, E., Novitch, B.G., and Huber, A.B. (2011). Npn-1 contributes to axon-axon interactions that differentially control sensory and motor innervation of the limb. PLoS Biol *9*, e1001020.

Ji, S.J., and Jaffrey, S.R. (2012). Intra-axonal translation of SMAD1/5/8 mediates retrograde regulation of trigeminal ganglia subtype specification. Neuron *74*, 95-107.

Kadkhodaei, B., Alvarsson, A., Schintu, N., Ramskold, D., Volakakis, N., Joodmardi, E., Yoshitake, T., Kehr, J., Decressac, M., Bjorklund, A*., et al.* (2013). Transcription factor Nurr1 maintains fiber integrity and nuclear-encoded mitochondrial gene expression in dopamine neurons. Proc Natl Acad Sci U S A *110*, 2360-2365.

Kalmar, B., Innes, A., Wanisch, K., Kolaszynska, A.K., Pandraud, A., Kelly, G., Abramov, A.Y., Reilly, M.M., Schiavo, G., and Greensmith, L. (2017). Mitochondrial deficits and abnormal mitochondrial retrograde axonal transport play a role in the pathogenesis of mutant Hsp27-induced Charcot Marie Tooth Disease. Hum Mol Genet *26*, 3313-3326.

Kar, A.N., Vargas, J.N.S., Chen, C.Y., Kowalak, J.A., Gioio, A.E., and Kaplan, B.B. (2017). Molecular determinants of cytochrome C oxidase IV mRNA axonal trafficking. Mol Cell Neurosci *80*, 32-43.

Kenna, K.P., van Doormaal, P.T., Dekker, A.M., Ticozzi, N., Kenna, B.J., Diekstra, F.P., van Rheenen, W., van Eijk, K.R., Jones, A.R., Keagle, P*., et al.* (2016). NEK1 variants confer susceptibility to amyotrophic lateral sclerosis. Nat Genet *48*, 1037-1042.

Kim, D., Langmead, B., and Salzberg, S.L. (2015). HISAT: a fast spliced aligner with low memory requirements. Nat Methods *12*, 357-360.

Kwiatkowski, T.J., Bosco, D., Leclerc, A., Tamrazian, E., Vanderburg, C., Russ, C., Davis, A., Gilchrist, J., Kasarskis, E., and Munsat, T. (2009). Mutations in the FUS/TLS gene on chromosome 16 cause familial amyotrophic lateral sclerosis. Science *323*, 1205-1208.

Lasek, R.J., Garner, J.A., and Brady, S.T. (1984). Axonal transport of the cytoplasmic matrix. J Cell Biol *99*, 212s-221s.

Lawrence, M., Huber, W., Pages, H., Aboyoun, P., Carlson, M., Gentleman, R., Morgan, M.T., and Carey, V.J. (2013). Software for computing and annotating genomic ranges. PLoS Comput Biol *9*, e1003118.

Lee, S.K., and Hollenbeck, P.J. (2003). Organization and translation of mRNA in sympathetic axons. J Cell Sci *116*, 4467-4478.

Lin, Y.C., and Koleske, A.J. (2010). Mechanisms of synapse and dendrite maintenance and their disruption in psychiatric and neurodegenerative disorders. Annu Rev Neurosci *33*, 349-378.

Litman, P., Barg, J., Rindzoonski, L., and Ginzburg, I. (1993). Subcellular localization of tau mRNA in differentiating neuronal cell culture: implications for neuronal polarity. Neuron *10*, 627-638.

Love, M.I., Huber, W., and Anders, S. (2014). Moderated estimation of fold change and dispersion for RNA-seq data with DESeq2. Genome Biol *15*, 550.

Lyabin, D.N., Doronin, A.N., Eliseeva, I.A., Guens, G.P., Kulakovskiy, I.V., and Ovchinnikov, L.P. (2014a). Alternative forms of Y-box binding protein 1 and YB-1 mRNA. PLoS One *9*, e104513.

Lyabin, D.N., Eliseeva, I.A., and Ovchinnikov, L.P. (2014b). YB-1 protein: functions and regulation. Wiley interdisciplinary reviews RNA *5*, 95-110.

McIntyre, J.C., Titlow, W.B., and McClintock, T.S. (2010). Axon growth and guidance genes identify nascent, immature, and mature olfactory sensory neurons. J Neurosci Res *88*, 3243-3256.

Mi, H., Huang, X., Muruganujan, A., Tang, H., Mills, C., Kang, D., and Thomas, P.D. (2017). PANTHER version 11: expanded annotation data from Gene Ontology and Reactome pathways, and data analysis tool enhancements. Nucleic Acids Res *45*, D183-d189.

Mills, R., Taylor-Weiner, H., Correia, J.C., Agudelo, L.Z., Allodi, I., Kolonelou, C., Martinez-Redondo, V., Ferreira, D.M.S., Nichterwitz, S., Comley, L.H.*, et al.* (2018). Neurturin is a PGC-1alpha1-controlled myokine that promotes motor neuron recruitment and neuromuscular junction formation. Mol Metab *7*, 12-22.

Minis, A., Dahary, D., Manor, O., Leshkowitz, D., Pilpel, Y., and Yaron, A. (2014). Subcellular transcriptomics-dissection of the mRNA composition in the axonal compartment of sensory neurons. Dev Neurobiol *74*, 365-381.

Naumann, M., Pal, A., Goswami, A., Lojewski, X., Japtok, J., Vehlow, A., Naujock, M., Gunther, R., Jin, M., Stanslowsky, N.*, et al.* (2018). Impaired DNA damage response signaling by FUS-NLS mutations leads to neurodegeneration and FUS aggregate formation. Nature communications *9*, 335.

Nichterwitz, S., Chen, G., Aguila Benitez, J., Yilmaz, M., Storvall, H., Cao, M., Sandberg, R., Deng, Q., and Hedlund, E. (2016). Laser capture microscopy coupled with Smart-seq2 for precise spatial transcriptomic profiling. Nat Commun *7*, 12139.

Picelli, S., Bjorklund, A.K., Faridani, O.R., Sagasser, S., Winberg, G., and Sandberg, R. (2013). Smart-seq2 for sensitive full-length transcriptome profiling in single cells. Nature methods *10*, 1096-1098.

Renton, A.E., Majounie, E., Waite, A., Simón-Sánchez, J., Rollinson, S., Gibbs, J.R., Schymick, J.C., Laaksovirta, H., Van Swieten, J.C., and Myllykangas, L. (2011). A hexanucleotide repeat expansion in C9ORF72 is the cause of chromosome 9p21-linked ALS-FTD. Neuron *72*, 257-268.

Rosen, D.R., Siddique, T., Patterson, D., Figlewicz, D.A., Sapp, P., Hentati, A., Donaldson, D., Goto, J., O'Regan, J.P., and Deng, H.-X. (1993). Mutations in Cu/Zn superoxide dismutase gene are associated with familial amyotrophic lateral sclerosis.

Rotem, N., Magen, I., Ionescu, A., Gershoni-Emek, N., Altman, T., Costa, C.J., Gradus, T., Pasmanik-Chor, M., Willis, D.E., Ben-Dov, I.Z.*, et al.* (2017). ALS Along the Axons - Expression of Coding and Noncoding RNA Differs in Axons of ALS models. Sci Rep *7*, 44500.

Saal, L., Briese, M., Kneitz, S., Glinka, M., and Sendtner, M. (2014). Subcellular transcriptome alterations in a cell culture model of spinal muscular atrophy point to widespread defects in axonal growth and presynaptic differentiation. RNA *20*, 1789-1802.

Sgado, P., Alberi, L., Gherbassi, D., Galasso, S.L., Ramakers, G.M., Alavian, K.N., Smidt, M.P., Dyck, R.H., and Simon, H.H. (2006). Slow progressive degeneration of nigral dopaminergic neurons in postnatal Engrailed mutant mice. Proc Natl Acad Sci U S A *103*, 15242-15247.

Sharma, S., Grintsevich, E.E., Hsueh, C., Reisler, E., and Gimzewski, J.K. (2012). Molecular cooperativity of drebrin1-300 binding and structural remodeling of F-actin. Biophys J *103*, 275-283.

Sreedharan, J., Blair, I.P., Tripathi, V.B., Hu, X., Vance, C., Rogelj, B., Ackerley, S., Durnall, J.C., Williams, K.L., and Buratti, E. (2008). TDP-43 mutations in familial and sporadic amyotrophic lateral sclerosis. Science *319*, 1668-1672.

Sugiyama, S., Di Nardo, A.A., Aizawa, S., Matsuo, I., Volovitch, M., Prochiantz, A., and Hensch, T.K. (2008). Experience-dependent transfer of Otx2 homeoprotein into the visual cortex activates postnatal plasticity. Cell *134*, 508-520.

Swinnen, B., and Robberecht, W. (2014). The phenotypic variability of amyotrophic lateral sclerosis. Nat Rev Neurol *10*, 661-670.

Szklarczyk, D., Franceschini, A., Wyder, S., Forslund, K., Heller, D., Huerta-Cepas, J., Simonovic, M., Roth, A., Santos, A., Tsafou, K.P.*, et al.* (2015). STRING v10: protein-protein interaction networks, integrated over the tree of life. Nucleic Acids Res *43*, D447-452.

Taylor, A.M., Berchtold, N.C., Perreau, V.M., Tu, C.H., Li Jeon, N., and Cotman, C.W. (2009). Axonal mRNA in uninjured and regenerating cortical mammalian axons. J Neurosci *29*, 4697-4707.

Taylor, A.M., Blurton-Jones, M., Rhee, S.W., Cribbs, D.H., Cotman, C.W., and Jeon, N.L. (2005). A microfluidic culture platform for CNS axonal injury, regeneration and transport. Nature methods *2*, 599-605.

Telley, L., Cadilhac, C., Cioni, J.M., Saywell, V., Jahannault-Talignani, C., Huettl, R.E., Sarrailh-Faivre, C., Dayer, A., Huber, A.B., and Ango, F. (2016). Dual Function of NRP1 in Axon Guidance and Subcellular Target Recognition in Cerebellum. Neuron *91*, 1276-1291.

Torero Ibad, R., Rheey, J., Mrejen, S., Forster, V., Picaud, S., Prochiantz, A., and Moya, K.L. (2011). Otx2 promotes the survival of damaged adult retinal ganglion cells and protects against excitotoxic loss of visual acuity in vivo. J Neurosci *31*, 5495-5503.

Tung, Y.T., Lu, Y.L., Peng, K.C., Yen, Y.P., Chang, M., Li, J., Jung, H., Thams, S., Huang, Y.P., Hung, J.H.*, et al.* (2015). Mir-17~92 Governs Motor Neuron Subtype Survival by Mediating Nuclear PTEN. Cell Rep *11*, 1305-1318.

Upadhyay, A., Amanullah, A., Chhangani, D., Mishra, R., Prasad, A., and Mishra, A. (2016). Mahogunin Ring Finger-1 (MGRN1), a Multifaceted Ubiquitin Ligase: Recent Unraveling of Neurobiological Mechanisms. Mol Neurobiol *53*, 4484-4496.

Valdez, G., Tapia, J.C., Lichtman, J.W., Fox, M.A., and Sanes, J.R. (2012). Shared resistance to aging and ALS in neuromuscular junctions of specific muscles. PLoS One *7*, e34640.

Vance, C., Rogelj, B., Hortobágyi, T., De Vos, K.J., Nishimura, A.L., Sreedharan, J., Hu, X., Smith, B., Ruddy, D., and Wright, P. (2009). Mutations in FUS, an RNA processing protein, cause familial amyotrophic lateral sclerosis type 6. Science *323*, 1208-1211.

Wichterle, H., Lieberam, I., Porter, J.A., and Jessell, T.M. (2002). Directed differentiation of embryonic stem cells into motor neurons. Cell *110*, 385-397.

Wizenmann, A., Brunet, I., Lam, J., Sonnier, L., Beurdeley, M., Zarbalis, K., Weisenhorn-Vogt, D., Weinl, C., Dwivedy, A., Joliot, A.*, et al.* (2009). Extracellular Engrailed participates in the topographic guidance of retinal axons in vivo. Neuron *64*, 355-366.

Yoon, B.C., Jung, H., Dwivedy, A., O'Hare, C.M., Zivraj, K.H., and Holt, C.E. (2012). Local translation of extranuclear lamin B promotes axon maintenance. Cell *148*, 752-764.

Zhang, Y., Chen, K., Sloan, S.A., Bennett, M.L., Scholze, A.R., O'Keeffe, S., Phatnani, H.P., Guarnieri, P., Caneda, C., Ruderisch, N.*, et al.* (2014). An RNA-sequencing transcriptome and splicing database of glia, neurons, and vascular cells of the cerebral cortex. J Neurosci *34*, 11929-11947.

Zhuang, B., Su, Y.S., and Sockanathan, S. (2009). FARP1 promotes the dendritic growth of spinal motor neuron subtypes through transmembrane Semaphorin6A and PlexinA4 signaling. Neuron *61*, 359-372.

Zuko, A., Oguro-Ando, A., Post, H., Taggenbrock, R.L., van Dijk, R.E., Altelaar, A.F., Heck, A.J., Petrenko, A.G., van der Zwaag, B., Shimoda, Y.*, et al.* (2016). Association of Cell Adhesion Molecules Contactin-6 and Latrophilin-1 Regulates Neuronal Apoptosis. Front Mol Neurosci *9*, 143.

FIGURES LEGENDS

Fig. 1 Axon-seq of motor axons in single microfluidic devices. (A,B) Anti-GFP immunofluorescence visualizes motor axons crossing the microgrooves and extending into the axonal compartment. MN somas are visualized with Hb9::eGFP and Isl1/2 staining. **(C,D)** Presence of Tau (Mapt) but very little Map2 indicates that mainly axons and not dendrites cross over into the other compartment. **(E)** Overview of the used methodology. MNs were cultured in one compartment of the microfluidic device and axons were recruited across microgrooves using a gradient of trophic factors. Compartments were separately lysed and cDNA libraries prepared for RNA sequencing. **(F)** Hb9::eGFP expression reveals that the somatic chamber is not affected by lysis of the axons. **(G)** The axonal fraction contained around 5,000 unique transcripts, while MN somas contained > 15,000 (mean ± SEM). **(H)** PCA based on all expressed genes showing 'contaminated' axon samples with an intermediate amount of detected genes that cluster away from the clean axon samples and towards the somatodendritic samples. **(I)** Expression of selected marker genes in soma and axon samples of this study and data from studies by Rotem et al. (2017) and Briese et al. (2016). Our clean axon samples separate from the rest, while axon and soma samples from previously published studies intermingled, indicating cross-contamination. Scale bars: **A:** 500 µm. **B:** 100 µm, also applies to **C** and **D**. **F:** 100 µm.

Fig. 2 Axons have a distinct transcriptome from somas. (A) PCA of all expressed genes revealed a clear separation of axons and somas. **(B)** Top 20 genes determining PC1-negative loading. All of them are strongly enriched in axons compared to somas. **(C-H)** Gene set enrichment analysis (GSEA) using fold changes from the DESeq2 differential expression output ranked list between axons and somas, without a p-value cut-off. GSEA uncovered pathways related to mitochondrial oxidative energy production, local translation and nonsense-mediated decay. Subdividing the oxidative energy production class into mitochondrial- and nuclear-encoded transcripts reveals an axonal enrichment for both. Differential expression was performed on the 5 axon samples that passed QC and 13 soma samples, as visualized in panels **A** and **B**. **(I)** Expression levels of the highest expressed transcripts in axons related to oxidative energy production. All of the genes plotted are significantly enriched in the axonal compartment compared to the somatodendritic compartment. P-values are derived from the DESeq2 differential expression and were adjusted for multiple testing. Data is represented as mean ± SEM. **(J)** Immunocytochemistry of Cox6a1, the most abundant mRNA in axons involved in energy production.

Fig. 3 A unique transcription factor repertoire localizes to axons (A) Of the top 50 highest expressed transcription factors in the soma and axon (at least 4 axonal samples), 16 overlapped. **(B)** Heatmap of expression values of transcription factors from panel A. **(C)** Top 10 transcription factors with the highest expression in axons. 5 were significantly enriched in axons, while 1 was enriched in somas. P-values are derived from differential expression between the 5 axon and 13 soma samples that passed QC and are corrected for multiple testing (mean ± SEM). **(D)** Immunocytochemistry for Ybx1, the most abundant transcription factor at mRNA level in axons.

Fig. 4 Cross-comparison between datasets reveals a core axonal transcriptome signature (A) Overlap between the top 5,000 most highly expressed transcripts in axons from 4 datasets. 1,750 genes are present in all 4 datasets, possibly providing a core signature for the axonal transcriptome. **(B)** GO term analysis for biological processes based on the 1,750 genes overlapping between all datasets revealed energy production, translation, vesicle processing/transport and mRNA splicing as enriched. **(C)** STRING analysis for protein-interactions of the 396 genes overlapping only between the motor axon samples showed distinct gene clusters involved in ribogenesis, vesicle transport and mRNA splicing.

Fig. 5 Overexpression of SOD1^{G93A} induces changes in the axonal transcriptome. (A) Staining for SOD1 and misfolded SOD1 in MN cultures. In SOD1^{G93A} expressing cells high levels of both SOD1 and misfSOD1 are detected, whereas no misfSOD1 is detected in control cells. **(B,C)** Expression levels of mouse SOD1 and human transgenic SOD1. Mouse SOD1 is enriched in axons, while transgenic human SOD1 is equally divided over both compartments. Levels of hSOD1 are approximately 10-fold higher in somas than mouse SOD1. Data is represented as mean ± SEM. **(D)** Heatmap of differentially expressed genes between 5 control axon samples and 4 axon samples from SOD1^{G93A} overexpressing MNs. A total of 121 genes were differentially expressed, of which 25 enriched in control axons and 96 in SOD1^{G93A} axons. **(E)** Selected differentially expressed genes from the analysis visualized in panel **D** with relevance to ALS and general neuronal functioning. All p-values are derived from the DESeq2 output and are corrected for multiple testing (mean ± SEM). **(F)** Overlap between dysregulated genes upon SOD1^{G93A} expression in our dataset and Smn knockdown in data from Saal et al. *(Saal et al., 2014)*. 16 genes are commonly dysregulated. 1 gene, Nrp1, is commonly downregulated.

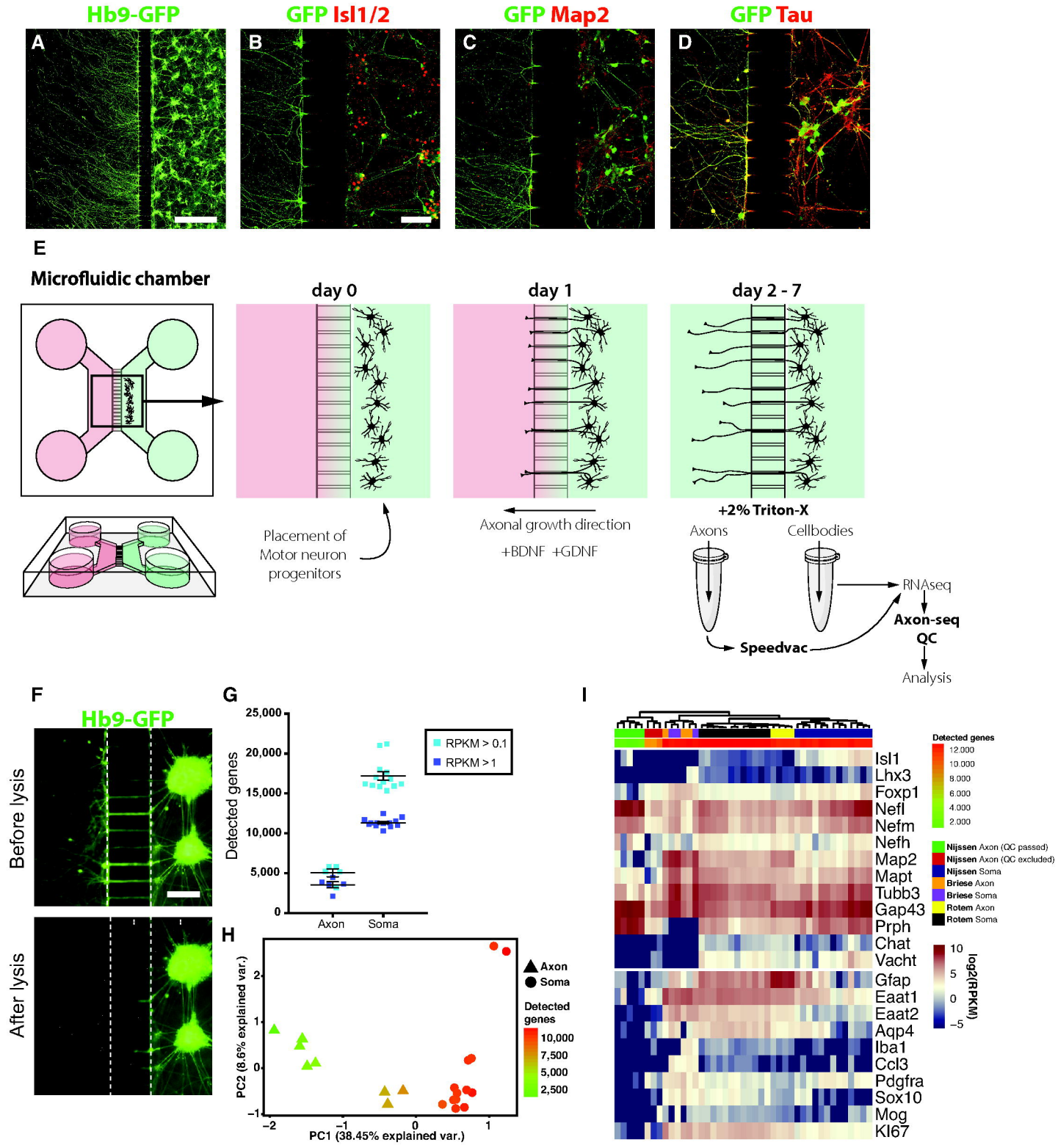
Hb9-GFP
GFP Isl1/2
GFP Map2
GFP Tau
A
B
C
D
E
Microfluidic chamber
day 0
day 1
day 2 - 7
Placement of Motor neuron progenitors
Axonal growth direction
+BDNF +GDNF
+2% Triton-X
Axons
Cellbodies
RNAseq
Axon-seq
QC
Speedvac
Analysis
F
Hb9-GFP
Before lysis
After lysis
G
Detected genes
RPKM > 0.1
RPKM > 1
Axon
Soma
H
PC2 (8.6% explained var.)
PC1 (38.45% explained var.)
Axon
Soma
Detected genes
10,000
7,500
5,000
2,500
I
Detected genes
Nijssen Axon (QC passed)
Nijssen Axon (QC excluded)
Nijssen Soma
Briese Axon
Briese Soma
Rotem Axon
Rotem Soma
log2(RPKM)
Isl1
Lhx3
Foxp1
Nefl
Nefm
Nefh
Map2
Mapt
Tubb3
Gap43
Prph
Chat
Vacht
Gfap
Eaat1
Eaat2
Aqp4
Iba1
Ccl3
Pdgfra
Sox10
Mog
KI67

Figure 1

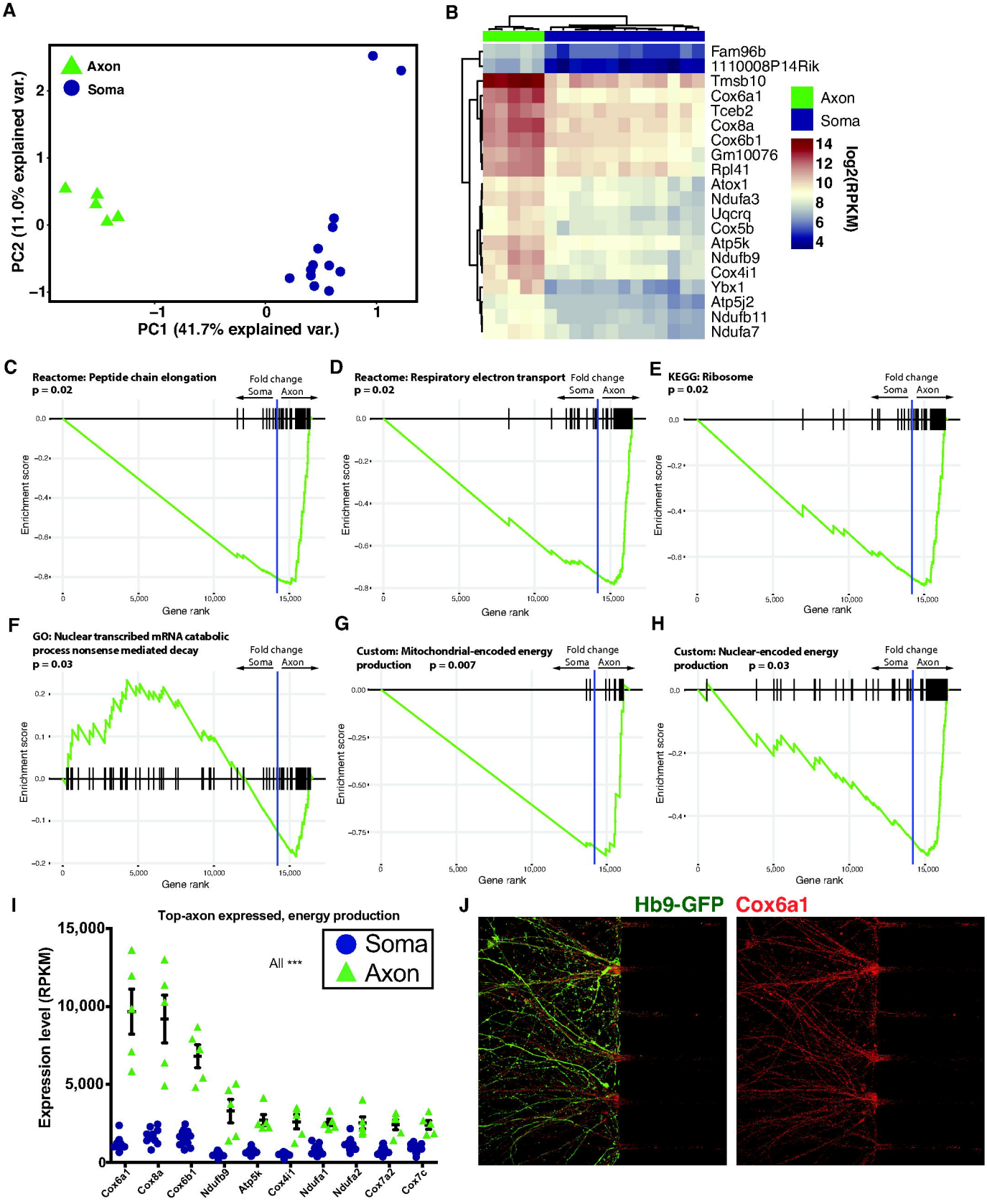
A
Axon
Soma
PC2 (11.0% explained var.)
PC1 (41.7% explained var.)
B
Fam96b
1110008P14Rik
Tmsb10
Cox6a1
Tceb2
Cox8a
Cox6b1
Gm10076
Rpl41
Atox1
Ndufa3
Uqcrq
Cox5b
Atp5k
Ndufb9
Cox4i1
Ybx1
Atp5j2
Ndufb11
Ndufa7
Axon
Soma
log2(RPKM)
C
Reactome: Peptide chain elongation
p = 0.02
D
Reactome: Respiratory electron transport
p = 0.02
E
KEGG: Ribosome
p = 0.02
F
GO: Nuclear transcribed mRNA catabolic process nonsense mediated decay
p = 0.03
G
Custom: Mitochondrial-encoded energy production p = 0.007
H
Custom: Nuclear-encoded energy production p = 0.03
Fold change
Soma
Axon
Enrichment score
Gene rank
I
Top-axon expressed, energy production
All ***
Soma
Axon
Expression level (RPKM)
Cox6a1
Cox8a
Cox6b1
Ndufb9
Atp5k
Cox4i1
Ndufa1
Ndufa2
Cox7a2
Cox7c
J
Hb9-GFP
Cox6a1

Figure 2

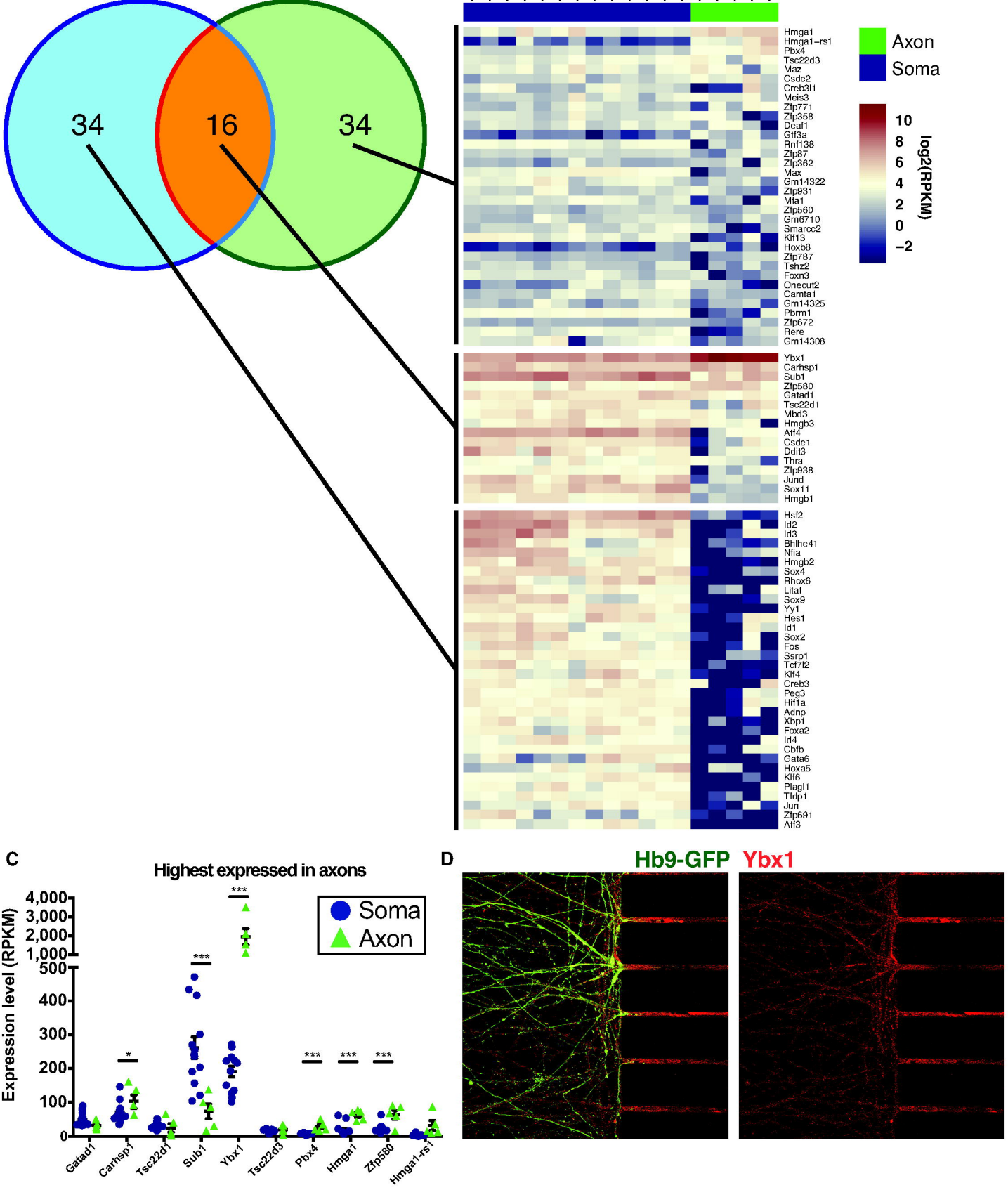
34
16
34
Axon
Soma
log2(RPKM)
10
8
6
4
2
0
−2
Hmga1
Hmga1−rs1
Pbx4
Tsc22d3
Maz
Csdc2
Creb3l1
Meis3
Zfp771
Zfp358
Deaf1
Gtf3a
Rnf138
Zfp87
Zfp362
Max
Gm14322
Zfp931
Mta1
Zfp560
Gm6710
Smarcc2
Klf13
Hoxb8
Zfp787
Tshz2
Foxn3
Onecut2
Camta1
Gm14325
Pbrm1
Zfp672
Rere
Gm14308
Ybx1
Carhsp1
Sub1
Zfp580
Gatad1
Tsc22d1
Mbd3
Hmgb3
Atf4
Csde1
Ddit3
Thra
Zfp938
Jund
Sox11
Hmgb1
Hsf2
Id2
Id3
Bhlhe41
Nfia
Hmgb2
Sox4
Rhox6
Litaf
Sox9
Yy1
Hes1
Id1
Sox2
Fos
Ssrp1
Tcf7l2
Klf4
Creb3
Peg3
Hif1a
Adnp
Xbp1
Foxa2
Id4
Cbfb
Gata6
Hoxa5
Klf6
Plagl1
Tfdp1
Jun
Zfp691
Atf3
C
Highest expressed in axons
Soma
Axon
Expression level (RPKM)
4,000
3,000
2,000
1,000
500
400
300
200
100
0
*
***
***
***
***
***
Gatad1
Carhsp1
Tsc22d1
Sub1
Ybx1
Tsc22d3
Pbx4
Hmga1
Zfp580
Hmga1-rs1
D
Hb9-GFP
Ybx1

Figure 3

A

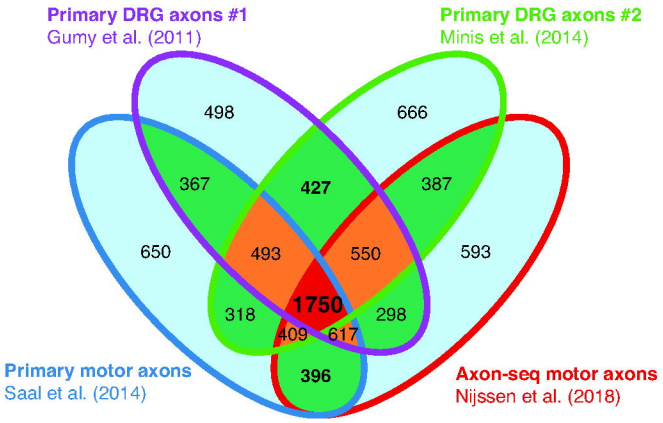

B

GO terms - Biological process (n = 1,750 genes)	# of genes (detected/total)	Enrichment score	Adj. p
Translational initiation	33/57	7.24	0.001
Vesicle budding from membrane	21/41	6.40	0.001
Anterograde axonal transport	13/30	5.42	0.01
Oxidative phosphorylation	25/61	5.21	0.001
Regulation of synaptic vesicle cycle	16/41	4.88	0.003
Proteasome-mediated ubiquitin-dependent protein catabolic process	72/235	3.83	0.001
Microtubule-based transport	35/124	3.53	0.001
mRNA splicing, via spliceosome	41/166	3.09	0.001

C

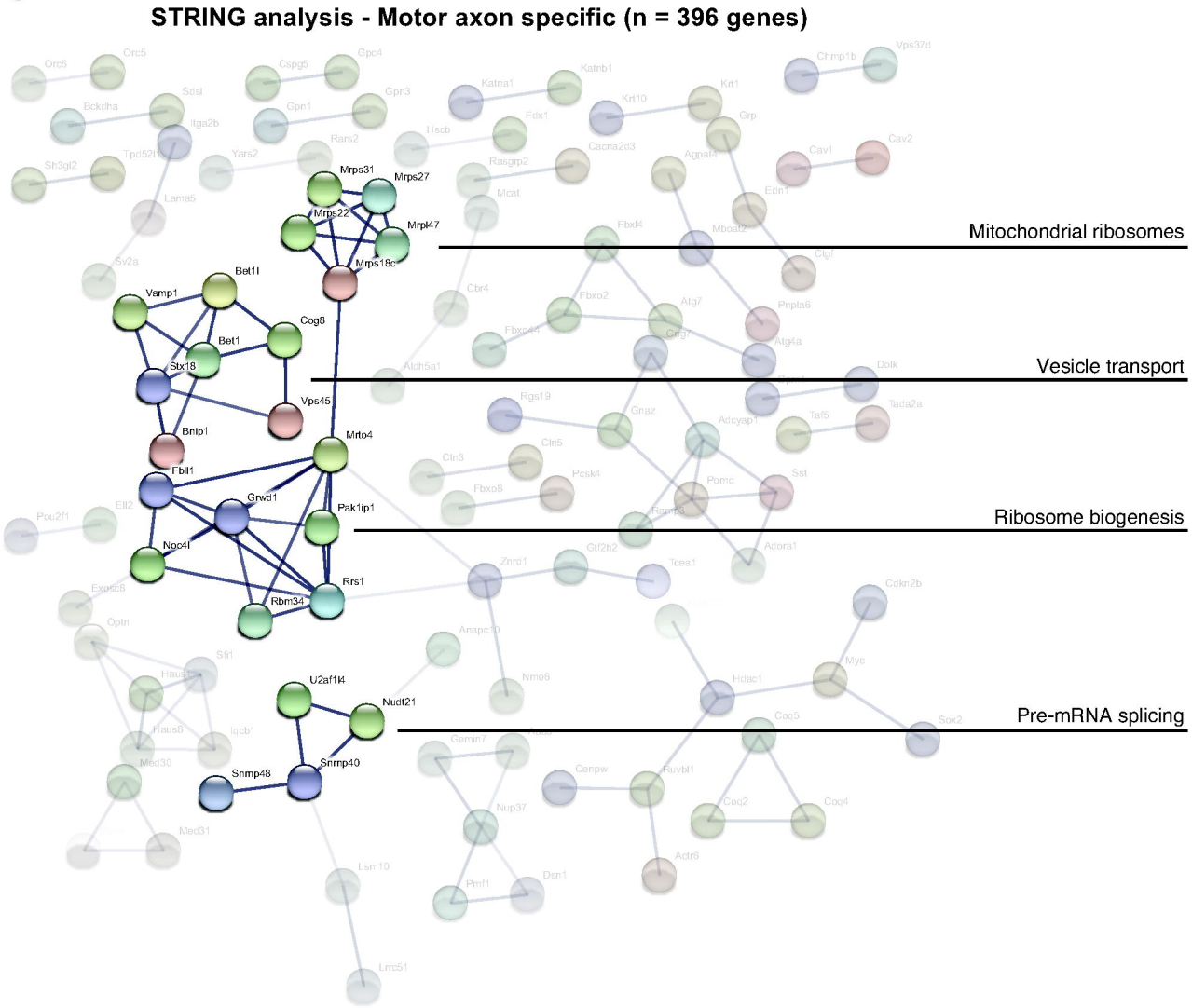

Figure 4

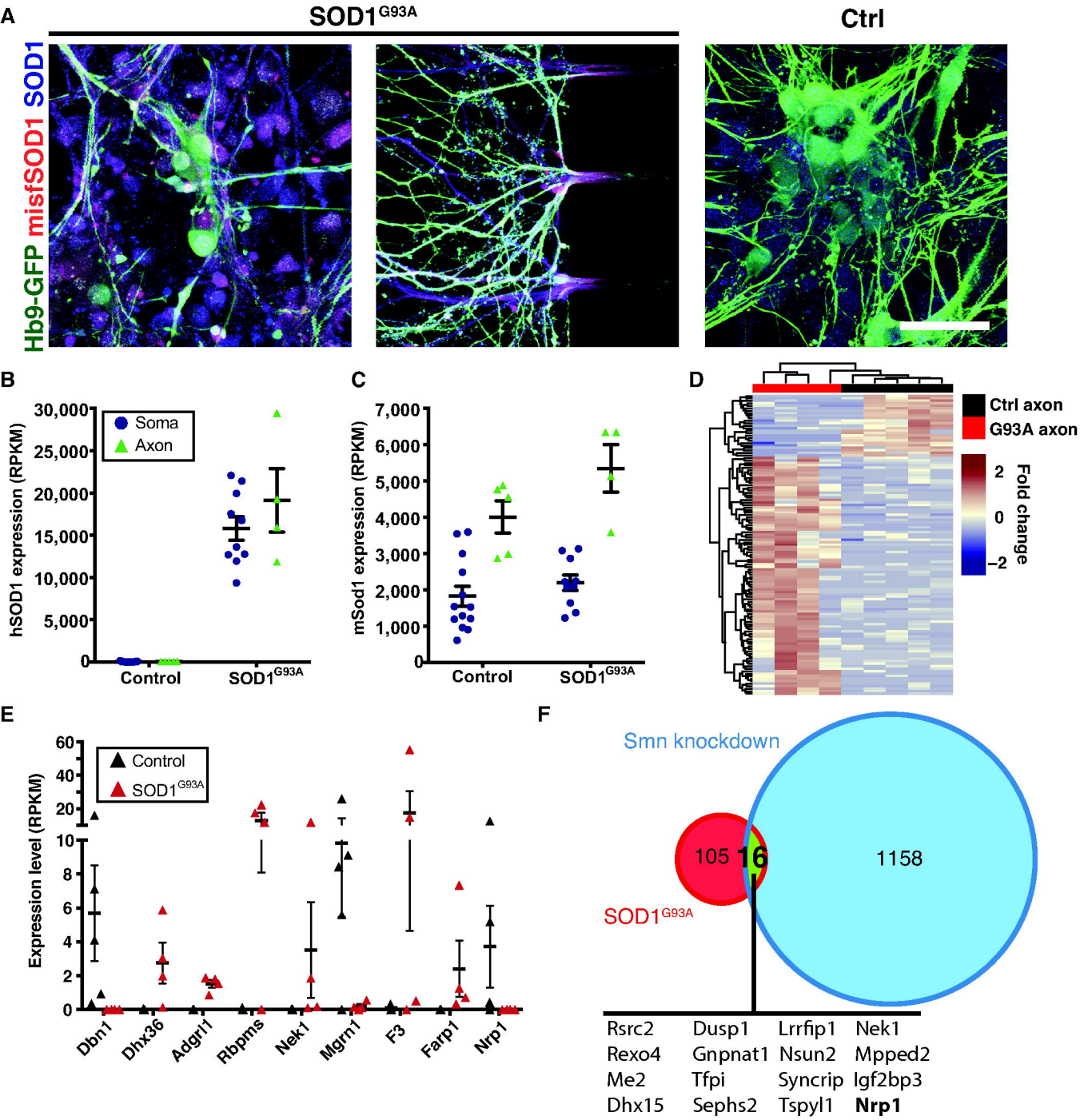
A
SOD1G93A
Ctrl
Hb9-GFP misfSOD1 SOD1
B
hSOD1 expression (RPKM)
Soma
Axon
Control
SOD1G93A
C
mSod1 expression (RPKM)
Control
SOD1G93A
D
Ctrl axon
G93A axon
Fold change
E
Expression level (RPKM)
Control
SOD1G93A
Dbn1
Dhx36
Adgrl1
Rbpms
Nek1
Mgrn1
F3
Farp1
Nrp1
F
Smn knockdown
105
16
1158
SOD1G93A
Rsrc2 Dusp1 Lrrfip1 Nek1
Rexo4 Gnpnat1 Nsun2 Mpped2
Me2 Tfpi Syncrip Igf2bp3
Dhx15 Sephs2 Tspyl1 Nrp1

Figure 5